Identification and Characterization of Mg^{2+} Binding Sites in Isolated α and β Subunits of H^+-ATPase from *Bacillus* PS3

Jean-Luc Zimmermann,*,‡ Toyoki Amano,§ and Claude Sigalat‡

CEA/Saclay, Département de Biologie Cellulaire et Moléculaire, Section de Bioénergétique, Bât. 532, F-91191 Gif-sur-Yvette, France, and Department of Biology and Geosciences, Shizuoka University, Shizuoka 422-8529, Japan

Received May 11, 1999; Revised Manuscript Received August 9, 1999

ABSTRACT: The properties of the nucleotide binding sites in the isolated β and α subunits of H^+-ATPase from *Bacillus* PS3 (TF1) have been examined by studying the EPR properties of bound VO^{2+}, which is a paramagnetic probe for the native Mg^{2+} cation cofactor. The amino acid ligands of the VO^{2+} complexes with the isolated β subunit, with the isolated α subunit, with different mixtures of both α and β subunits, and with the catalytic $\alpha_3\beta_3\gamma$ subcomplex have been characterized by a combination of EPR, ESEEM, and HYSCORE spectroscopies. The EPR spectrum of the isolated β subunit with bound VO^{2+} (1 VO^{2+}/β) is characterized by ^{51}V hyperfine coupling parameters ($A_{\|} = 168 \times 10^{-4}$ cm^{-1} and $A_{\perp} = 60 \times 10^{-4}$ cm^{-1}) that suggest that VO^{2+} binds to the isolated β subunit with at least one nitrogen ligand. Results obtained for the analogous VO^{2+} complex with the isolated α subunit are virtually identical. ESEEM and HYSCORE spectra are also reported and are similar for both complexes, indicating a very similar coordination scheme for VO^{2+} bound to isolated α and β subunits. In the isolated β (or α) subunit, the bound VO^{2+} cation is coordinated by one nitrogen ligand with hyperfine coupling parameters $A_{\|}(^{14}N) = 4.44$ MHz, and $A_{\perp}(^{14}N) = 4.3$ MHz and quadrupole coupling parameters $e^2qQ \approx 3.18$ MHz and $\eta \approx 1$. These are typical for amine-type nitrogen ligands equatorial to the VO^{2+} cation; amino acid residues in the TF1 β and α subunits with nitrogen donors that may bind VO^{2+} are reviewed. VO^{2+} bound to a mixture of α and β subunits in the presence of 200 mM Na_2SO_4 to promote the formation of the $\alpha_3\beta_3$ hexamer has a second nitrogen ligand with magnetic properties similar to those of a histidine imidazole. This situation is analogous to that in the $\alpha_3\beta_3\gamma$ subcomplex and in the whole TF1 enzyme [Buy, C., Matsui, T., Andrianambinintsoa, S., Sigalat, C., Girault, G., and Zimmermann, J.-L. (1996) *Biochemistry 35,* 14281−14293]. These data are interpreted in terms of only partially structured nucleotide binding sites in the isolated β and α subunits as compared to fully structured nucleotide binding sites in the $\alpha_3\beta_3$ heterohexamer, the $\alpha_3\beta_3\gamma$ subcomplex, and the whole TF1 ATPase.

H^+-ATP synthase plays a central role in energy conversion in bacteria, mitochondria, and chloroplasts and uses a transmembrane proton gradient to generate ATP[1] from ADP and inorganic phosphate (*1, 2*). The enzyme is a multisubunit complex made of a membrane-spanning domain F0 that transports protons and a soluble extrinsic catalytic domain F1. Dissipation of the proton gradient through the F0 domain is coupled to the synthesis of ATP in the catalytic F1 domain: the current view proposes that the energy from the proton gradient is first converted into mechanical energy that induces rotation of the γ subunit in the F1 catalytic part, thereby furnishing the conformational energy necessary for the synthesis of ATP (*1, 2*). The unidirectional rotation of the γ subunit of F1 has actually been observed under some conditions (*3*−*6*).

Isolated F1 has an ATP hydrolyzing activity, and its five different protein subunits ($\alpha_3\beta_3\gamma\epsilon$) have highly conserved amino acid sequences between different sources. The F1 ATPase from the thermophilic bacterium *Bacillus* PS3 (TF1) has a molecular mass of 385 000 Da (*7*), and the properties of the isolated α and β subunits (*8, 9*) and of the $\alpha_3\beta_3$ and $\alpha_3\beta_3\gamma$ subcomplexes (*10*−*14*) have been studied quite extensively. The crystal structure of the nucleotide-free $\alpha_3\beta_3$ subcomplex shows that the oligomer of approximate spherical shape with 100 Å diameter has exact 3-fold symmetry with the six alternating α and β subunits arranged like the segments of an orange (*14*). In the crystal structure of the homologous bovine MF1 ATPase, a pseudo-3-fold symmetry axis is relating the α and β subunits that contain five bound nucleotides (*15*) so that the conformation of the α and β subunits is different from that seen in the TF1 $\alpha_3\beta_3$ subcomplex, but the overall structure is similar.

The F1 ATPase contains six nucleotide binding sites among which three are catalytic and participate in the phosphorylation reaction and three are noncatalytic with

* To whom correspondence should be addressed. Tel: +33 1 69 08 68 39. Fax: +33 1 69 08 87 17. E-mail: jean-luc.zimmermann@cea.fr.

‡ CEA/Saclay.

§ Shizuoka University.

[1] Abbreviations: ADP, adenosine 5′-diphosphate; AMPPNP, adenosine 5′-(β,γ-imido)triphosphate; ATP, adenosine 5′-triphosphate; CF1, F1 ATPase from chloroplast; CW, continuous wave; EDTA, ethylenediaminetetraacetic acid; EPR, electron paramagnetic resonance or, equivalently, electron spin resonance or ESR; ESEEM, electron spin−echo envelope modulation; FT, Fourier transform; HPLC, high-performance liquid chromatography; HYSCORE, hyperfine sublevel correlation spectroscopy; MF1, F1 ATPase from bovine heart mitochondria; TF1, F1 ATPase from thermophilic *Bacillus* PS3.

10.1021/bi9910732 CCC: $18.00
Published on Web 10/26/1999

much less clear function (*16*). These nucleotide binding sites are located at the interfaces between the α and β subunits, with the catalytic sites being formed by residues mostly from the β subunits and the three other noncatalytic sites essentially formed by residues on the α subunits (*15*). Both the ATP synthesis and hydrolysis reactions necessitate the presence of divalent metal cations, and in the MF1 crystal structure, this is manifest as Mg^{2+} cations associated with either the ADP or AMPPNP nucleotide molecules in the five nucleotide binding sites that are occupied. Depending on the presence of ADP or AMPPNP in the nucleotide site, the Mg^{2+} ion is coordinated by one or two phosphate oxygens from the nucleotides. The various possible functional roles for this divalent metal cation may include optimally orienting the polyphosphate chain in the active site, shielding of the negative charges on the coordinated phosphate(s), assisting the formation of the negative charge on the leaving group, and coordinating nonbridging phosphate oxygens to stabilize the pentacovalent transition state (*17*−*19*).

Apart from the phosphate oxygens, ligands derived from amino acid residues in the α and β subunits are also involved in binding the Mg^{2+} cofactors. In fact, the MF1 crystal structure has identified the hydroxyl group of β-Thr163 as coordinating the Mg^{2+} in the β_{DP} and β_{TP} sites, i.e., the two catalytic sites with bound nucleotides (*15*). In addition, it has also been shown that in these sites the more distant β-Glu188 and β-Asp256 have carboxylate oxygens also involved in binding the Mg^{2+}, perhaps by polarizing direct water ligands (*20*), a situation that is beyond observation in the available crystal structure. These conserved amino acids correspond to β-Thr165, β-Glu190, and β-Asp252 in TF1.

In the MF1 crystal structure, the three noncatalytic α_E, α_{DP}, and α_{TP} sites appear to be very similar to each other in terms of Mg^{2+} binding. All three sites are occupied by an AMPPNP molecule associated with a Mg^{2+} cation, and the latter is coordinated by two oxygen atoms from the β and γ phosphates of the nucleotide and the hydroxyl oxygen of α-Thr176, which is the β-Thr163 homologue on the α subunit (*15*). It is possible that the carboxylate group of α-Asp269 with oxygen atoms at ≈3 Å from the Mg^{2+} is also involved in the coordination of the Mg^{2+}.

The coordination of the divalent metal cation in F1 and possible changes occurring in the course of catalysis may be probed using paramagnetic analogues of the native Mg^{2+} including Mn^{2+} and VO^{2+}. Not unexpectedly, six binding sites for Mn^{2+} have been determined on F1 using EPR spectroscopy (*21*). On the other hand, the vanadyl cation VO^{2+} has been shown to be an effective paramagnetic substitute for many divalent metal ions in metalloproteins and metalloenzymes. It is particularly useful for probing Ca^{2+} and Mg^{2+} sites (*22*), for which few direct investigation techniques are available. Using the EPR and ESEEM properties of VO^{2+} bound to F1, two binding sites with high affinity have been reported in the chloroplast CF1 enzyme that involve one amine ligand each from a lysine side chain (*23*). These lysine ligands were identified with those present in the nucleotide binding sites (*24*), and they correspond in TF1 to α-Lys175 and β-Lys164, respectively. VO^{2+} bound to metal-depleted TF1 in stoichiometric conditions was recently shown to be coordinated by two different nitrogen ligands that were proposed as an amine nitrogen and an imidazole nitrogen based on their hyperfine and quadrupole coupling parameters determined by ESEEM and HYSCORE (*25*). A similar coordination scheme was found for VO^{2+} bound to the TF1 subcomplex $\alpha_3\beta_3\gamma$, and the amine ligand to the unique bound VO^{2+} was also proposed to correspond to the side chain of β-Lys164 (*25*).

In the present work, the binding of VO^{2+} as probe for the native Mg^{2+} has been studied in the isolated β and α subunits of TF1 in an attempt to possibly identify the origin of the two nitrogen ligands for VO^{2+} bound in the nucleotide site formed by the interface of the α and β subunits in TF1. Using EPR, ESEEM, and HYSCORE spectroscopies, the binding of VO^{2+} to the isolated α and β subunits is shown to involve only one nitrogen ligand that corresponds to the amine ligand of VO^{2+} bound to the whole TF1. The additional VO^{2+} ligand that was previously identified in $\alpha_3\beta_3\gamma$ and TF1 is observed only upon formation of the $\alpha_3\beta_3$ subcomplex from a mixture of the individual α and β subunits. These results are interpreted using the structural data available for bovine MF1 and the $\alpha_3\beta_3$ subcomplex of TF1: It is suggested that these reflect differences in the accessibility and/or geometry of the nucleotide binding sites in the isolated α and β subunits, the $\alpha_3\beta_3$ hexamer, the $\alpha_3\beta_3\gamma$ subcomplex, or the whole TF1 enzyme. This emphasizes the role of the β/α interface including residues from the catalytic β subunit but also from the neighboring α subunit directly or indirectly involved in the design of fully active catalytic sites. Alternatively, these data may reflect conformational changes at the nucleotide binding site in the β subunit induced by the β−α protein−protein interaction.

MATERIALS AND METHODS

The α and β subunits of TF1 were overexpressed in *Escherichia coli* strain DK8 and purified as described previously (*26*). The βH119Q mutant was prepared and purified as described (*27*) and was a kind gift from Prof. Akutsu.

The recombinant $\alpha_3\beta_3\gamma$ subcomplex was prepared by using the expression plasmids of the α, β, and γ subunits in *E. coli* and was purified as described (*13*).

For the preparation of EPR samples of the isolated α and β subunits with bound VO^{2+}, typically 4 mg of the polypeptide as precipitate in $(NH_4)_2SO_4$ was solubilized in 150 μL of 50 mM HEPES−NaOH, pH 7, and the desired amount of VO^{2+} was added from a solution of $VOSO_4$ in 200 mM sodium maleate at pH 6.3. The mixture was transferred in a quartz EPR tube and immediately frozen in liquid N_2. The EPR sample with the $\alpha_3\beta_3\gamma$ subcomplex was prepared in an analogous way. In some instances, the protein precipitate was first dialyzed in 50 mM HEPES−NaOH, 10 mM EDTA (pH 7), and then 50 mM HEPES−NaOH (pH 7) before addition of VO^{2+}. No difference in the EPR properties of VO^{2+} was found between the two sample preparations. Mixtures of the α and β subunits were prepared by first mixing precipitates of the two polypeptides followed by solubilization in 150 μL of 50 mM HEPES−NaOH (pH 7) with or without 200 mM Na_2SO in order to control the formation of the $\alpha_3\beta_3$ heterohexamer (*10*). EPR samples with VO^{2+} bound with glycinate or imidazole were prepared as described previously (*25*).

Titration of VO^{2+} bound to the β subunit was done by measuring the amplitude of the VO^{2+} EPR signal at low

temperature in a sample of the β subunit supplemented with increasing amounts of VO^{2+}. The VO^{2+} concentration in the $VOSO_4$ stock solution was determined using electronic absorption ($\epsilon_{750\,nm} = 18\ M^{-1}\ cm^{-1}$; *22*) and was crossed-checked by atomic absorption spectroscopy of vanadium. The molar concentration of the β subunit was determined using the method of Bradford with the Bio-Rad protein assay and MW = 52 kDa. Calibration of the EPR signal vs concentration of bound VO^{2+} was performed using samples with increasing concentrations of VO^{2+} complexed with imidazole. The good linear relationship between the concentration of VO^{2+} in these samples and the size of the EPR signal then allowed the determination of bound VO^{2+} in the β samples.

The degree of association of the α and β subunits in the EPR samples was characterized with HPLC using a TSK G3000 SW gel filtration column as previously described (*12*). The column was equilibrated with a buffer identical to that used for the EPR sample.

EPR spectra at X band were recorded with a Bruker 200D spectrometer equipped with a microwave frequency counter (Hewlett-Packard 5350B) and a NMR gaussmeter (Bruker ER035M). Spectra were recorded at liquid helium temperatures using an Oxford Instruments cryostat. Simulations of the EPR spectra were performed using perturbation theory to second order as described previously (*28*).

1D-ESEEM and 2D-HYSCORE data were recorded with a Bruker ER380E pulsed EPR spectrometer. For the 1D-ESEEM experiments, the amplitude of the stimulated echo ($\pi/2-\tau-\pi/2-T-\pi/2-\tau-$echo) is monitored as a function of time T with τ as a fixed parameter. The τ values (see figure legends) were chosen to minimize the contribution of weakly coupled protons to the echo modulation. The time domain data were processed as previously described to yield the frequency domain ESEEM spectra (*25*). The 2D-HYSCORE experiments were performed using the 4-pulse sequence $\pi/2-\tau-\pi/2-t_1-\pi-t_2-\pi/2$ and monitoring the inverted echo occurring at time τ after the last microwave pulse (*29*). The experimental details were as described in ref *25*, except that for each data set the length and power of the $\pi/2$ and π pulses were each individually adjusted to optimize the inversion of the spin−echo. A typical 200 × 200 data array obtained by incrementing t_1 and t_2 with Δt = 16 ns was processed and Fourier transformed as described previously (*25*). The results in this paper are presented as contour plots after Fourier transformation and magnitude calculation. Connectivities between nuclear frequencies appear in two different quadrants referred to as the positive (f_1, f_2) and negative ($-f_1$, f_2) quadrants. The 'skyline projection' 1D spectra shown in the figures are the projections of the 2D connectivities along each of the frequency axes.

RESULTS

The CW EPR spectrum of the β subunit supplemented with a stoichiometric amount of VO^{2+} (1 VO^{2+}/β) is shown in Figure 1 (trace a) together with its simulation (trace b). This spectrum is representative of the VO^{2+} cation in an axial environment and the EPR parameters that best fit the spectrum ($g_\perp = 1.983$, $A_\perp(^{51}V) = 60 \times 10^{-4}\ cm^{-1}$, $g_\parallel = 1.945$, $A_\parallel(^{51}V) = 168 \times 10^{-4}\ cm^{-1}$) show the typically reduced $A_\parallel$ hyperfine coupling constant that is observed when VO^{2+} is coordinated with nitrogen ligands (*22*). In addition, these EPR parameters are very similar to those found for VO^{2+} complexes with the whole TF1 enzyme and with the $\alpha_3\beta_3\gamma$ subcomplex (*25*). In these two instances, it was demonstrated that VO^{2+} is bound to the protein with two nitrogen ligands (*25*). This indicates that, for the isolated β subunit, the added VO^{2+} binds at a site that involves at least one nitrogen ligand.

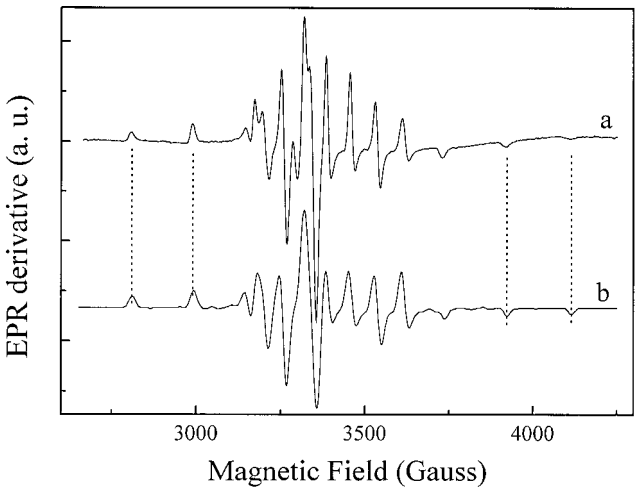

FIGURE 1: (Trace a): X band CW EPR spectrum of the TF1 β subunit supplemented with VO^{2+} (1 VO^{2+}/β). Experimental conditions are as follows: temperature, 4.2 K; microwave power, 0.2 mW; microwave frequency, 9.4362 GHz; modulation amplitude, 10 G. (Trace b): Simulation of the spectrum in trace a using the following parameters: $g_\perp = 1.983$, $A_\perp(^{51}V) = 60 \times 10^{-4}\ cm^{-1}$, $g_\parallel = 1.945$, $A_\parallel(^{51}V) = 168 \times 10^{-4}\ cm^{-1}$, and a 12 G-width Gaussian derivative line.

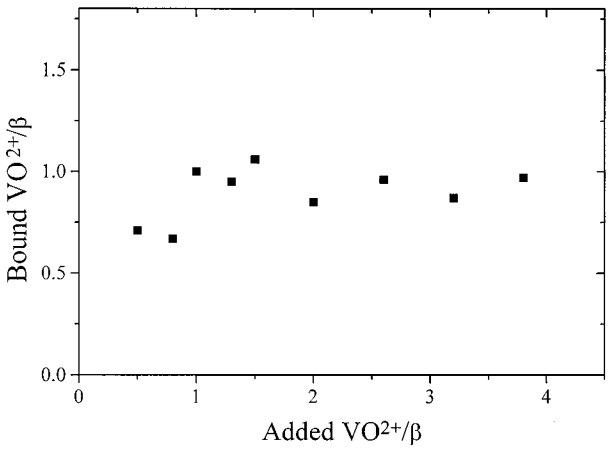

FIGURE 2: Binding of VO^{2+} to the isolated β subunit as a function of the added VO^{2+} concentration. The amount of bound VO^{2+} was measured as the amplitude of the EPR signal measured as in Figure 1a.

To evaluate the possible existence of other VO^{2+} binding sites in the isolated β subunit, the amplitude of the VO^{2+} EPR signal was measured for samples of the β subunit supplemented with increasing amounts of VO^{2+}. Figure 2 shows that the VO^{2+} EPR signal in the β sample measured in the conditions of Figure 1a increases up to added VO^{2+}/β ratios of approximately 1, after which further additions of VO^{2+} do not produce any increase in the VO^{2+} EPR signal. These results indicate that, under these conditions, no more than one metal binding site can be filled with VO^{2+} in the isolated β.

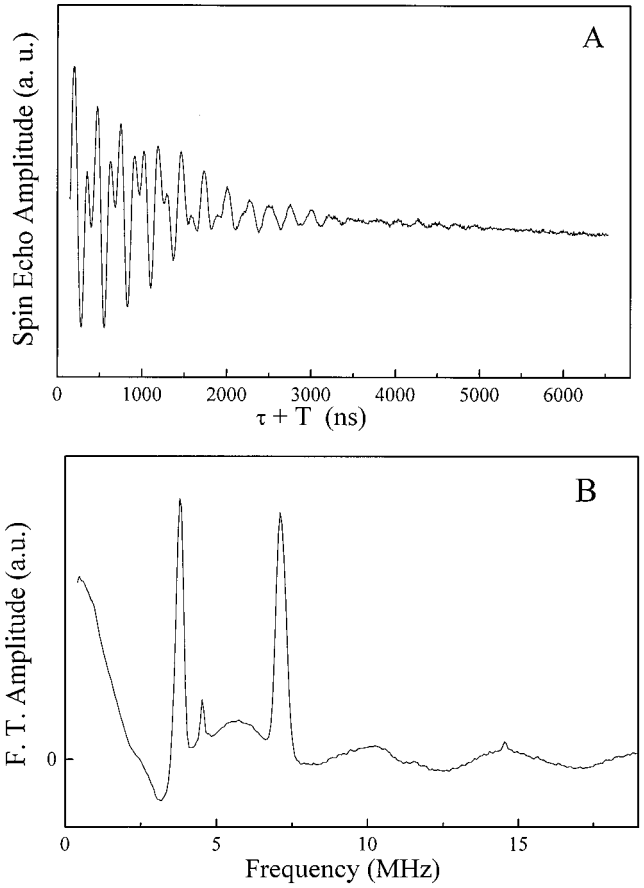

FIGURE 3: Three-pulse ESEEM (panel A) and corresponding FT (panel B) of VO^{2+} bound to β (1 VO^{2+}/β). The data were obtained with a sample temperature of 5.0 K, a microwave frequency of 9.63 GHz, and a magnetic field setting of 3427 G. The interpulse time τ was 136 ns, and the time interval between successive pulse sets was 1.54 ms.

To evaluate the nature of the nitrogen ligand(s) in the β subunit that is involved in binding the VO^{2+} cation, ESEEM spectra were measured for a sample of isolated β (1 VO^{2+}/β). Figure 3 shows the 3-pulse ESEEM signal (panel A) and its Fourier transform (panel B) measured with an external magnetic field of 3427 G, corresponding to the absorption maximum in the CW EPR spectrum. The ESEEM spectrum, which is dominated by two intense frequency components at ≈3.88 and 7.17 MHz, is reminiscent of a spin system with a coupled ^{14}N nucleus ($I = 1$) with small hyperfine anisotropy. The observed frequencies correspond to the two $\nu_{dq\pm}$ 'double-quantum' nuclear frequencies ($\Delta M_I = 2$) of ^{14}N (*30, 31*). Figure 4A shows a plot of the two frequencies in Figure 3B as a function of the magnetic field. In this experiment, the 3-pulse ESEEM signal was recorded with the magnetic field strength set between ≈2900 and 4200 G. The straight lines in Figure 4A represent the fits to eq 1, which relates the two double-quantum frequencies $\nu_{dq\pm}$ to the hyperfine coupling constant A, the quadrupole coupling constant $4K = e^2qQ$, and the asymmetry parameter η (*30, 31*):

$$\nu_{dq\pm} = 2[(\nu_L \pm (A/2))^2 + K^2(3 + \eta^2)]^{1/2} \qquad (1)$$

using $A = 4.44$ MHz, $e^2qQ = 3.10$ MHz, and $\eta = 1$ (solid lines) and $A = 4.3$ MHz, $e^2qQ = 3.10$ MHz, and $\eta = 1$ (dotted lines). In this equation, ν_L is the Larmor frequency of ^{14}N.

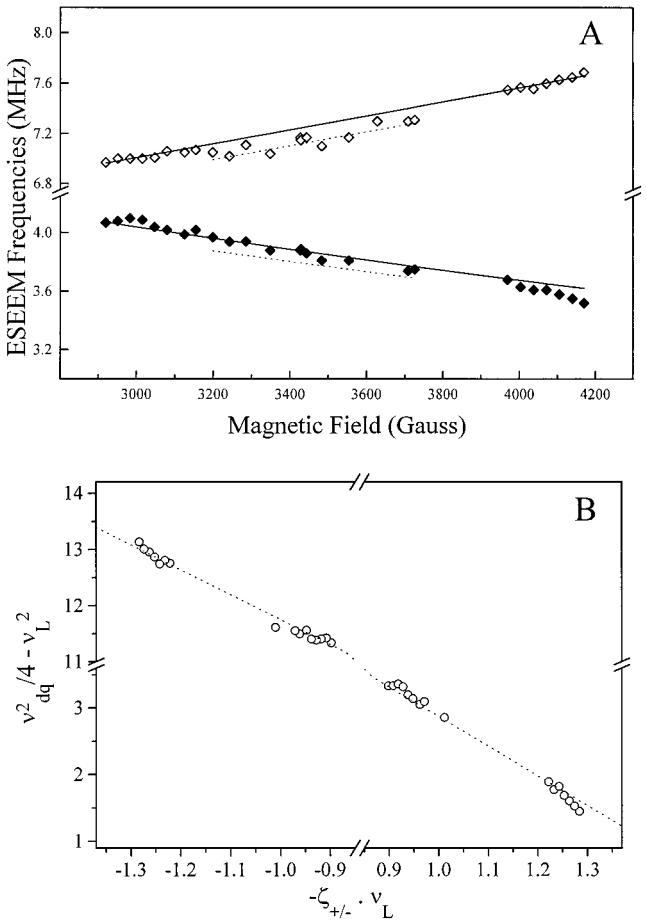

FIGURE 4: (Panel A): Plots of the ESEEM frequencies observed for VO^{2+} bound to the isolated β subunit as a function of the external magnetic field. The straight lines are fits to the data points using $\nu_{dq\pm} = 2[(\nu_L \pm (A/2))^2 + K^2(3 + \eta^2)]^{1/2}$ and the following parameters: $A = 4.44$ MHz, $e^2qQ = 4K = 3.10$ MHz, $\eta = 1$ (solid lines) and $A = 4.3$ MHz, $e^2qQ = 3.10$ MHz, $\eta = 1$ (dashed lines). (Panel B): Plots of $(\nu_{dq}^2/4 - \nu_L^2)$ as a function of $-\zeta_\pm\nu_L$. $\nu_{dq\pm}$ are the two double-quantum frequencies of the ^{14}N coordinating the VO^{2+}, ν_L is the Larmor frequency of ^{14}N, and $\zeta_\pm$ is the sign of the $M_S = \pm 1/2$ in the manifold associated with $\nu_{dq\pm}$.

To obtain the coupling parameters A, K, and η that fit eq 1 with the experimental points, the data in Figure 4A were first plotted as $\nu_{dq\pm}^2/4 - \nu_L^2$ as a function of $-\zeta_\pm\nu_L$, where $\zeta_\pm$ is the sign of M_S in the manifold associated with $\nu_{dq\pm}$ (see ref *25*). In fact, by rearranging eq 1 as

$$\frac{\nu_{dq\pm}^2}{4} - \nu_L^2 = \mp A\nu_L + \frac{A^2}{4} + K^2(3 + \eta^2) \qquad (2)$$

A is given by the slope of the fit of $\nu_{dq\pm}^2/4 - \nu_L^2$ vs $-\zeta_\pm\nu_L$, and $K^2(3 + \eta^2)$ is obtained as the origin of the abscissa. Figure 4B shows the plot of $\nu_{dq\pm}^2/4 - \nu_L^2$ vs $-\zeta_\pm\nu_L$ obtained for the data points corresponding to $H \parallel z$, i.e., below ≈3150 G and above ≈3900 G. This partial set of data is informative because due to the large anisotropy of the ^{51}V hyperfine tensor, the resonant spin packets involve those paramagnets with the axial direction of the ^{51}V hyperfine tensor, i.e., the V═O molecular axis, parallel to the external magnetic field. Therefore, the ^{14}N hyperfine coupling A that best fits these data is assigned to the parallel $A_\parallel$ hyperfine component. The data points obtained for other magnetic field values can be fitted with $A = 4.3$ MHz which is assigned to $A_\perp$ (dashed lines).

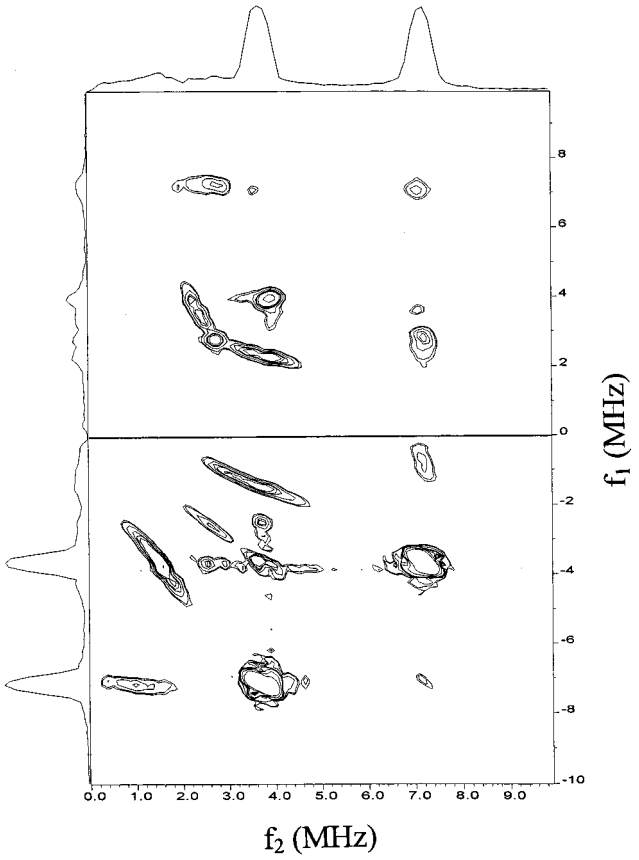

FIGURE 5: 2D-HYSCORE spectra (contour plots and skyline projections) of VO^{2+} bound to β. Experimental conditions were as follows: temperature, 5.0 K; microwave frequency, 9.62 GHz; $f_1 \times f_2 = 200 \times 200$ points; starting times, $t_1 = t_2 = 80$ ns; time increments, $\Delta t_1 = \Delta t_2 = 16$ ns; $\tau = 192$ ns; shot repetition time, 1.54 ms; and magnetic field, 3432 G.

Information on nuclear couplings can also be obtained using the HYSCORE pulse sequence. For VO^{2+} complexes, 2D-HYSCORE spectra have been shown to yield correlations between nuclear transitions of coupled ^{14}N and ^{31}P nuclei (*25*, *32*, *33*). In particular, for complexes of VO^{2+} with TF1 or its subcomplex $\alpha_3\beta_3\gamma$, correlations between the two $\nu_{dq\pm}$ of each of two different ^{14}N ligands could be observed in the negative quadrant of the contour plot (*25*). Figure 5 shows the HYSCORE contour plot obtained for the β sample with one added VO^{2+}. The observation of the strong correlations at ≈(3.7, −7.2) and (7.2, −3.7) MHz in the negative quadrant confirms the assignment of the 3.7 and 7.2 MHz frequencies to the $\nu_{dq\pm}$ of a coupled ^{14}N. However, five additional correlations can be identified in the HYSCORE and also assigned to the coupling with the ^{14}N atom. First, the couple of features at ≈(1.0, −7.2) and (7.2, −1.0) MHz in the negative quadrant, and that at ≈(2.7, 7.2) and (7.2, 2.7) MHz in the positive quadrant both correlate $\nu_{dq+} \approx 7.2$ MHz with two frequencies whose sum $1.0 + 2.7 = 3.7$ corresponds to the second double-quantum frequency at $\nu_{dq-} = 3.7$ MHz. Consequently, the frequencies at 1.0 and 2.7 MHz are assigned to single quantum transitions of ^{14}N in the manifold associated with ν_{dq-}. The two couples of features that appear like ridges at ≈(2.6, 3.7) and ≈(3.7, 2.6) MHz in the positive quadrant and at ≈(1.5, −3.7) and ≈(−1.5, 3.7) MHz in the negative quadrant together with a mirror image of the former in the negative quadrant are all correlations involving the ν_{dq-} frequency and a second frequency associated with the other M_S manifold. No additivity relationship can be found here between these nuclear frequencies, probably due to the increased anisotropy affecting the nuclear transitions in this manifold. This anisotropy is also probably the origin of the pronounced ridge-like shape of the correlation features in the HYSCORE.

The identification of additional nuclear frequencies corresponding to the ^{14}N coupled to VO^{2+} bound to the isolated β subunit allows the determination of e^2qQ and η for this coupled nitrogen. To this end, the graphical method reported in ref *34* has been used to obtain values for K and η that reproduced best the nuclear frequencies obtained in the HYSCORE. After change for the dimensionless variables $\omega = \nu_{ef-}/K$ and $x = \nu/K$ where $\nu_{ef-} = (\nu_L - A/2)^2$, one considers the following mathematical function:

$$F(x) = 2\omega^{-2}(1-\eta^2) \pm \omega^{-2}3^{-3/2}[x^2 - x_c^2][4x_c^2 - x^2]^{1/2}$$

with $x_c = (\omega^2 + 3 + \eta^2)^{1/2}$.

The nuclear frequencies correspond to the values of x at which $g(\theta, \varphi)$ intersects $F(x)$ (*31*, *34*) with

$$g(\theta, \varphi) = 3\cos^2\theta - 1 + \eta\cos 2\theta \sin^2\theta$$

The graphical method yields $A = 4.44$ MHz, $e^2qQ = 4K = 3.18$ MHz, and $\eta = 1$. This in turn predicts three spectroscopic frequencies at $\nu_1 = 0.99$, $\nu_2 = 2.79$, and $\nu_3 = \nu_{dq-} = 3.78$ MHz, which are indeed quite close to the experimental HYSCORE frequencies.

As a support for the present interpretation, the HYSCORE spectrum was measured for a sample of VO^{2+} complexed with glycinate. In this solution complex, the echo modulation arises from the coupling with the glycinate amine nitrogen bound to the VO^{2+}. HYSCORE correlations are detected with frequencies at 1.5, 2.4, 3.9, and 7.8 MHz that can be analyzed within the same framework as above for the sample with the β subunit. The analysis yields $A = 4.80$ MHz, $e^2qQ = 3.20$ MHz, and $\eta = 1.00$. The similarity with both the hyperfine and quadrupole coupling parameters measured for the ^{14}N ligand in the β subunit is striking, suggesting that the binding site for VO^{2+} in the β subunit involves an amine nitrogen rather than an imidazole nitrogen for which substantially different coupling parameters are found ($A = 6.4$ MHz, $e^2qQ = 2.0-2.3$ MHz; *25*).

The binding of VO^{2+} has also been examined for the β mutant in which His119 is replaced by a glutamine. The EPR and ESEEM spectra of a mixture of VO^{2+} with this mutant βH119Q show no change in the binding of VO^{2+} as compared to the wild-type polypeptide, indicating that the His119 imidazole side chain is not the VO^{2+} ligand in the β subunit (not shown).

Three copies of the α subunit of TF1 are present in the catalytic TF1, forming in association with three copies of the β subunit the $\alpha_3\beta_3$ hexameric domain of TF1. The α subunit is therefore an important part of the enzyme. A significant aspect of the function of the α subunit is its involvement in the formation, at the β/α interfaces, of the nucleotide active sites involved in the binding change mechanism. In addition, the amino acid analysis of the α subunit shows that significant homologies exist between the α and β subunits. In the crystal structures of MF1 (*15*) and of the $\alpha_3\beta_3$ crown of TF1 (*14*), the nucleotide sites in the β

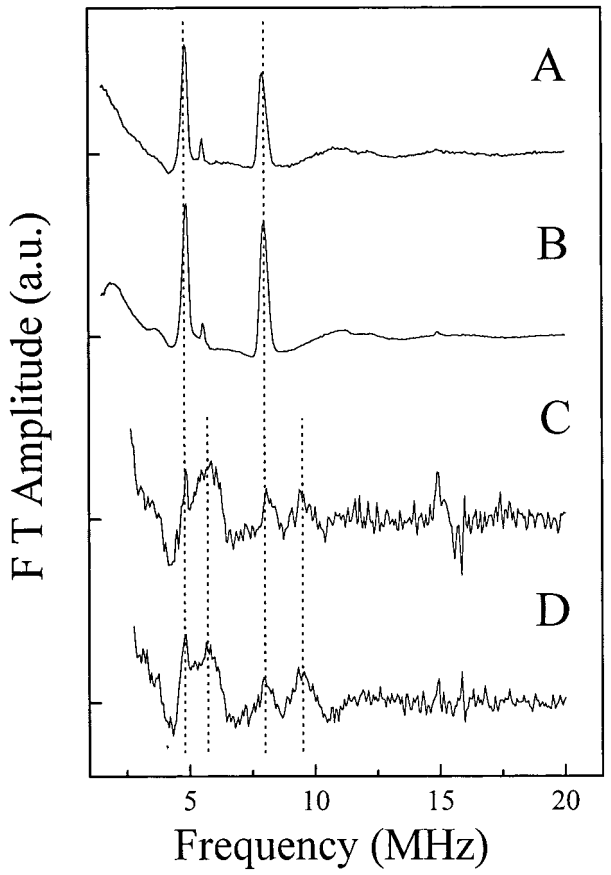

FIGURE 6: Three-pulse Fourier transform ESEEM spectra of stoichiometric VO^{2+} bound to the isolated α subunit (A), a stoichiometric mixture of the α and β subunits (B), the mixture of α and β subunits with 200 mM Na_2SO_4 (C), and the $\alpha_3\beta_3\gamma$ subcomplex (D). The data were recorded at $T = 5.0$ K with $\tau = 136$ ns and a magnetic field $H = 3430$ G. The dashed lines emphasize features that are similar in the spectra.

subunits have also significant homologies with those located in the α subunits. It is clear however that, despite these homologies, the β nucleotide sites are catalytic while those on the α subunits are not. It is therefore of major interest to determine the structural origin of this functional difference. To this end, we have studied the binding of VO^{2+} by the isolated α subunit and analyzed the EPR, ESEEM, and HYSCORE data of VO^{2+} bound to isolated α. In fact, the spectra of a 1:1 mixture of VO^{2+} and α were all virtually identical to those obtained for the β subunit and analyzed above (see Figure 6A). This result first demonstrates that VO^{2+} binds to the α subunit with a nitrogen ligand, similarly to the situation in the β subunit. Within the accuracy limit of the hyperfine and quadrupole coupling parameters derived from the HYSCORE spectra, these are identical for the ^{14}N ligand that binds the VO^{2+} in the isolated α and isolated β subunits. It is therefore highly probable that the amino acid that provides the ^{14}N ligand to the VO^{2+} is conserved between the α and β subunits.

The binding of VO^{2+} to the isolated α and β subunits is different from the binding of VO^{2+} to the whole TF1 enzyme and also to the $\alpha_3\beta_3\gamma$ subcomplex. In these latter two instances, both the ESEEM and HYSCORE data of stoichiometric mixtures with VO^{2+} indicated that the cation was coordinated with two nitrogen ligands characterized by two rather different hyperfine and quadrupole coupling parameters (*25*). The first ligand ^{14}N gave rise to an isotropic hyperfine coupling $|A| = 4.75$ MHz and a quadrupole coupling parameter e^2qQ between 2.8 and 3.2 MHz (*25*). The magnetic coupling parameters determined in the present study for the coupled ^{14}N from the isolated β and that from the isolated α are very similar. For both TF1 and the $\alpha_3\beta_3\gamma$ subcomplex, the binding site for VO^{2+} is located close to a nucleotide binding site, at a site that is normally filled with Mg^{2+}, and also a site that is probably catalytic and made of residues mostly from a β subunit (*25*). Thus, it is reasonable to suggest that the nitrogen ligand that coordinates VO^{2+} in the isolated β subunit is identical to the ligand with the same coupling parameters and that binds VO^{2+} in TF1 and in $\alpha_3\beta_3\gamma$. The second ^{14}N ligand to VO^{2+} identified both in TF1 and $\alpha_3\beta_3\gamma$ was characterized by a larger $|A| = 6.5$ MHz and a smaller e^2qQ (2.0−2.3 MHz), which were found typical for an imidazole nitrogen (*25*). Interestingly, this putative histidine ligand is absent in the VO^{2+} binding site of both the isolated α and β subunits.

The mode of binding of VO^{2+} has been studied in two different samples containing stoichiometric mixtures of the α and β subunits. A first sample was made by adding the α and β subunits in HEPES buffer (pH 7.0) with no further addition except the VO^{2+} solution (see Materials and Methods). A second sample was made in which 200 mM Na_2SO_4 was present throughout the different dialysis steps in order to stabilize the formation of the $\alpha_3\beta_3$ hexamer (*10*). The actual formation of the $\alpha_3\beta_3$ subcomplex in the EPR sample was confirmed by the observation of a single peak at the corresponding molecular weight in the HPLC elution profile of the sample made from the mixture of the α and β subunits in the presence of 200 mM Na_2SO_4 (not shown). The ESEEM spectra that were obtained for these samples prepared with VO^{2+} bound in stoichiometric amount are shown in Figure 6, panels B and C, together with those obtained for VO^{2+} bound to the isolated α subunit (Figure 6A) and the $\alpha_3\beta_3\gamma$ subcomplex (Figure 6D). It can immediately be seen that, for the $\alpha\beta$ mixture in the absence of Na_2SO_4, the ESEEM spectrum is virtually identical to that obtained for VO^{2+} bound to the isolated α subunit or to the isolated β subunit (Figure 3B). This is interpreted as indicating that no change in the coordination of VO^{2+}, at least in terms of nitrogen ligands, has occurred for this sample. By contrast, when 200 mM Na_2SO_4 is present with the equimolar mixture of α and β, the ESEEM spectrum of bound VO^{2+} shows four frequency peaks at 3.87, 4.80, 7.26, and 8.80 MHz, just like the spectrum of VO^{2+} bound to the $\alpha_3\beta_3\gamma$ subcomplex (panel D) or to the whole TF1 enzyme (Figure 2A in ref *25*). This first confirms that the $\alpha_3\beta_3$ subcomplex did assemble under these conditions and also indicates that a change of ligands occurred for the bound VO^{2+}. The similarity of the frequency peaks in the ESEEM spectrum of VO^{2+} bound to this $\alpha_3\beta_3$ subcomplex with that reported for TF1 and that for $\alpha_3\beta_3\gamma$ subcomplex indicates that the bound VO^{2+} is coordinated by two nitrogen ligands; the first one is identical to that in the isolated α and β subunits and the second one has coupling parameters similar to those of an imidazole nitrogen (*25*). It is also of note in Figure 6 that the ESEEM spectra for VO^{2+} bound to the $\alpha_3\beta_3$ and $\alpha_3\beta_3\gamma$ subcomplexes (panels C and D) are characterized by a much less signal-to-noise ratio than those for the VO^{2+} bound to the isolated α and β subunits (panels A and B), although the concentrations of protein and VO^{2+}

added in the four samples were comparable. The rather small ESEEM signals in panels C and D were in the present study related to correspondingly small echoes being observed in the time domain, indicating that only a small proportion of the added VO^{2+} did bind to the $\alpha_3\beta_3$ or $\alpha_3\beta_3\gamma$ samples, although stoichiometric amounts were added. However, adventitious and nonspecific binding of VO^{2+} to the $\alpha_3\beta_3$ and $\alpha_3\beta_3\gamma$ subcomplexes can be ruled out because the ESEEM frequencies (Figure 6C,D) are so similar to those measured for VO^{2+} bound to the whole TF1 for which the strong echo intensity and ESEEM signal indicate high-affinity binding (*25*). It is therefore concluded that, despite the differences in binding affinities, VO^{2+} binds to the same binding site in $\alpha_3\beta_3$, $\alpha_3\beta_3\gamma$, and TF1. In fact, this process is made possible because VO^{2+} is not stable at pH 7 in the absence of suitable ligands, and this suggests that the accessibility of VO^{2+} to the divalent metal binding site is lowered in the subcomplexes as compared to the isolated subunits, perhaps due to closing of the binding site by the adjacent subunit upon formation of the $\alpha_3\beta_3$ crown of the subcomplexes. An alternative possibility is that the affinity for the divalent metal cation is lowered in the $\alpha_3\beta_3$ and $\alpha_3\beta_3\gamma$ subcomplexes as compared to that in whole TF1 (see below). The signal-to-noise ratio of the ESEEM of VO^{2+} bound to TF1 (*25*) is in fact comparable to that measured for α and β and much larger than that observed here for the $\alpha_3\beta_3$ and the $\alpha_3\beta_3\gamma$ subcomplexes, suggesting a decreased accessibility of the VO^{2+} cation for the divalent metal binding site in the two subcomplexes compared to the whole TF1 enzyme.

DISCUSSION

VO^{2+} binds to the isolated β subunit from TF1 as demonstrated by the observation of an EPR spectrum with specific hyperfine coupling parameters for the stoichiometric complex $VO^{2+}\cdot\beta$ at pH 7. Because most of the protein ligands that build the catalytic nucleotide and divalent metal (Mg^{2+}) binding sites in TF1 belong to the β subunits, the VO^{2+} binding site that is shown in the present study for the β subunit when isolated is also probably the Mg^{2+} binding site on the β subunit. In fact, the isolated β subunit has been shown to bind nucleotides in the presence of Mg^{2+} cations (*35*), suggesting that binding sites for divalent metal cations also exist on isolated β. The identity of the VO^{2+} and Mg^{2+} binding sites in the isolated β subunit does not indicate that competition between the two cations can actually be observed: The stability constants of VO^{2+} complexes with ligands of biological significance are always at least 1000 times larger than those with Mn^{2+} (*22*), which in turn are generally higher than with Mg^{2+}. In fact, for a sample with 100 μM isolated β, the presence of 1 mM $MgCl_2$ did not prevent the observation of the EPR signal of bound VO^{2+} (not shown). For the isolated β with one VO^{2+} bound, the observation of a CW EPR spectrum with reduced hyperfine coupling constants is indicative of a binding site with nitrogen-based ligands. Furthermore, the ESEEM and HYSCORE data demonstrate that the bound VO^{2+} is coordinated by one nitrogen ligand with hyperfine coupling parameters $A_{\|}(^{14}N) = 4.44$ MHz and $A_{\perp}(^{14}N) = 4.3$ MHz and with quadrupole coupling parameters $e^2qQ \approx 3.18$ MHz and $\eta \approx 1$. In a previous study, we have discussed possible amino acid candidates for nitrogen-based ligands to bound VO^{2+} depending on their hyperfine and quadrupole coupling parameters (*25*). In particular, it was shown that an imidazole nitrogen ligand gives rise to a larger hyperfine coupling (≈6.4 MHz) and a smaller (2.0−2.3 MHz) quadrupole coupling parameter than those measured for the NH_2 group of glycinate bound to VO^{2+} ($A = 4.8$ MHz, $e^2qQ = 2.6-3.0$ MHz) (*25*). The latter example was taken as a representative for VO^{2+} coordinated by an amine group. The coupling parameters determined here with greater precision from the HYSCORE spectra for the nitrogen ligand in the VO^{2+} binding site in the β subunit are remarkably similar. Therefore, it is concluded that this VO^{2+} binding site involves an amine ligand. In addition, LoBrutto et al. (*36*) have shown that amine nitrogen ligands axial to the VO^{2+} are characterized by significantly smaller (≈1.3 MHz) hyperfine couplings than equatorial nitrogen ligands (≈5 MHz). This is taken as evidence that the amine ligand identified here for VO^{2+} bound to isolated β (and also to isolated α) is equatorial to the VO^{2+}. For the identification of the amino acid residue that provides this nitrogen ligand, the examination of the crystal structures available for the $\alpha_3\beta_3$ subcomplex of TF1 (*14*) and for the related MF1 enzyme (*15*) is informative. In fact, although the $\alpha_3\beta_3$ structure would probably be the most relevant structural model for the interpretation of the present spectroscopic data, the nucleotide and metal binding sites in the $\alpha_3\beta_3$ crystal are empty (except for the presence of the SO_4^{2-} anion, which seems to mimic a nucleotide β-phosphate), and this prevents any direct determination of the metal ion environment. It is however highly informative to realize that the structures of the nucleotide binding sites in the $\alpha_3\beta_3$ crown of TF1 are practically superimposable with the empty β_E site in the MF1 structure. The other two β-based nucleotide sites in MF1, β_{DP} and β_{TP}, each contain one Mg^{2+} ion associated with a nucleotide. A number of peptide nitrogen atoms are in close proximity to the Mg^{2+} in these β_{DP} and β_{TP} sites and may also be believed to bind the VO^{2+} when the nucleotide is absent and/or in the absence of the adjacent α subunit. The first candidate, which has also been proposed to bind VO^{2+} in TF1 and in the $\alpha_3\beta_3\gamma$ subcomplex (*25*), is the ε amine nitrogen of β-Lys164[2] that is located at distances of 5.20 Å in β_{DP} and 5.36 Å in β_{TP} from the Mg^{2+}. This lysine residue was also proposed to bind VO^{2+} in the chloroplast CF1 enzyme (*23*). Interestingly, the guanidinium nitrogens of the more distant β-Arg191 are also at relatively small distances (4.08, 5.74, and 6.33 Å in β_{DP}; 3.97, 5.88, and 6.02 Å in β_{TP}). Peptide N_α nitrogens may also serve as metal ligands in metalloproteins (see, e.g., ref *37*) and therefore need to be considered here. Among these, the N_α of β-Lys164 (5.70 Å in β_{DP} and 5.80 Å in β_{TP}) and the N_α of the adjacent P-loop residues β-Thr165 (4.09 Å in β_{DP} and 4.18 Å in β_{TP}) and β-Val166 (6.03 Å in β_{DP} and 6.05 Å in β_{TP}) are also reasonable candidates for binding the VO^{2+} cation under the present experimental conditions. It is of note that the γ amide nitrogen of β-Asn257 is located at 5.32 Å (5.45 Å) from the Mg^{2+} in the MF1 β_{DP} (β_{TP}) site, but since the asparagine is replaced for a methionine (Met253) in the β subunit from TF1, it cannot be considered for coordinating the VO^{2+} in the present study.

[2] Although the discussion is based on the MF1 crystal structure, the amino acid numbering relevant to the analogous TF1 enzyme is used here, which is the enzyme under study.

The spectroscopic data for VO^{2+} bound to the TF1 isolated α subunit are extremely similar to those reported above for the β subunit. Here, the candidate for the amine ligand to the metal cation may be found by examining, in the MF1 structure, the noncatalytic α_E, α_{DP}, and α_{TP} nucleotide binding sites that are all occupied by Mg^{2+} and the nucleotide inhibitor AMPPNP in the MF1 crystal (*15*). The protein nitrogen atoms located at distances shorter than 6 Å from the Mg^{2+} cation are the amine N_ϵ of α-Lys175 at ≈5 Å and the N_α of α-Lys175 (≈5.5 Å), of α-Thr176 (≈3 Å), and of α-Ser177 (≈5.9 Å) together with the δ amide nitrogen of α-Gln172 (≈5.9 Å). Rather interestingly, these amino acids, except for the glutamine, are the α homologues of those from the β subunit that are candidates for binding the VO^{2+} (β-Lys164, β-Thr165, and β-Val166). It is also of note that the three guanidinium nitrogens of β-Arg191 mentioned above have no counterpart on the α subunit. Due to the strong similarity of the spectroscopic data for the α and β subunits, this suggests that β-Arg191 can probably be excluded as the nitrogen ligand for the VO^{2+} in the isolated β and that binding of VO^{2+} by the isolated α and β subunits involves a nitrogen ligand that is conserved between the two homologous subunits. Therefore, it is concluded that the amino acid that provides a nitrogen ligand to VO^{2+} in the isolated β subunit of TF1 is β-Lys164 (ϵ-NH_2 or N_α), β-Thr165 (N_α), or β-Val166 (N_α). For the isolated α subunit the candidates are α-Lys175 (ϵ-NH_2 or N_α), α-Thr176 (N_α), and α-Ser177 (N_α).

Under conditions in which the $\alpha_3\beta_3$ hexamer assembles, i.e., in the presence of 200 mM Na_2SO_4 or in the presence of the additional γ subunit as in the $\alpha_3\beta_3\gamma$ subcomplex (*25*), VO^{2+} appears to bind in a manner similar to that observed in TF1: Two nitrogen ligands with two different spectroscopic signatures coordinate the VO^{2+} in a Mg^{2+} binding site. It is presently not clear, when stoichiometric conditions are used, whether the added VO^{2+} binds to a β or an α site. It was argued, for the whole TF1 enzyme and also for the $\alpha_3\beta_3\gamma$ subcomplex, that the site was a catalytic site located on the β subunit (*25*). The rationale is not valid for the $\alpha_3\beta_3$ subcomplex, since in the absence of the γ subunit, the three β sites are certainly equivalent as are also the α sites, and the relative affinities of the six sites for nucleotide and Mg^{2+} are not known. Therefore, both possibilities need to be considered for the interpretation of the present spectroscopic data.

A first possibility is that the additional nitrogen ligand to the bound VO^{2+} originates from the adjacent polypeptide subunit, i.e., the α subunit nearest to the catalytic site in a β subunit, or the β subunit nearest to the noncatalytic site in an α subunit. The examination of the catalytic β_{TP} and β_{DP} sites in MF1 shows that the only amino acid from the adjacent α subunit with nitrogen atoms at distances compatible with coordinating the VO^{2+} under our experimental conditions is α-Arg365. One of the three guanidinium nitrogens of this arginine is located at distances 5.01 Å from the Mg^{2+} in β_{TP} and at 4.72 Å in β_{DP}, i.e., at distances compatible with its involvement in binding the VO^{2+} cation. There are, however, several difficulties to firmly establish this interpretation. First, the coordination of a metal cation like VO^{2+} by a (deprotonated) derivative of the guanidinium group of an arginine residue is presently not documented. Second, the hyperfine and quadrupole coupling constants of the nitrogen atom in the putative resulting VO^{2+} complex are not known either. Further work in characterizing the EPR properties of VO^{2+} with ^{14}N ligands of different classes are needed to clarify this point. Quite interestingly, this interpretation cannot hold for VO^{2+} bound to an α site since the nearest nitrogen atom from a neighboring β subunit is located farther than 8.5 Å (β-Arg352).

An alternative possibility is that the differences in the binding of VO^{2+} to the isolated α and β subunits and to the $\alpha_3\beta_3$ and $\alpha_3\beta_3\gamma$ subcomplexes are manifest of considerable change that occurs in the conformation of the β and α subunits upon formation of the $\alpha_3\beta_3$ moiety. Although there is presently no structural data in the literature to substantiate this possibility, it certainly cannot be presently excluded, and it is rather illuminating to consider how such a ligand change could take place. Interestingly, one of the guanidinium nitrogens of β-Arg191, which is at 3.97 Å from the Mg^{2+} in the β_{TP} site (4.08 Å in β_{DP}), may play this role if the side chain is positioned away from the Mg^{2+} binding site in the isolated β. This interpretation is possible only for a β site since β-Arg191 has no counterpart in the α subunits. In the absence of structural data for the isolated α and β subunits, further discussion along these lines would probably be too speculative.

The situation of VO^{2+} bound to TF1 and the subcomplexes $\alpha_3\beta_3\gamma$ (*25*) and $\alpha_3\beta_3$ (this study) with two nitrogen ligands appears to be different from the situation reported for the analogous chloroplast enzyme CF1 (*23*). In this latter case, a single nitrogen ligand assigned to the side chain of the P-loop lysine was reported for VO^{2+} bound to a catalytic or noncatalytic site. Other differences include the presence of a strongly bound ADP and Mg^{2+} cation at a catalytic site in CF1, whereas TF1, its $\alpha_3\beta_3\gamma$ and $\alpha_3\beta_3$ subcomplexes, and the α and β subunits are completely devoid of nucleotide and Mg^{2+}; and the reported discrepancy regarding the enzymatic activation by VO^{2+} (*23*, *25*). Certainly these important differences between the two enzymes are also reflected in the mode of coordination for VO^{2+}, perhaps indicating that the second nitrogen ligand that is observed for TF1 may not be conserved in CF1.

CONCLUDING REMARKS

Taken together, the present spectroscopic results of VO^{2+} bound to the $\alpha_3\beta_3$ and $\alpha_3\beta_3\gamma$ subcomplexes and to the isolated α and β subunits of TF1 demonstrate that the binding of the bound cation is changed when the $\alpha_3\beta_3$ hexameric moiety is formed. Although it is presently difficult to firmly assess the structural origin of these differences, the ESEEM results indicate that, although the nucleotide binding sites, both catalytic and noncatalytic, are mostly made of residues from one subunit of the $\alpha_3\beta_3$ hexamer, the actual geometry of the nucleotide site in the active enzyme depends heavily on the formation of the hexamer perhaps via the direct participation of residues from the adjacent subunit and that some of these changes can be probed by EPR spectroscopy.

ACKNOWLEDGMENT

J.-L.Z. thanks Dr. Benoît Schneider for extremely useful discussions. We also thank Prof. Hideo Akutsu, Department of Bioengineering, Yokohama National University, Japan, for providing a sample of βH119Q.

REFERENCES

1. Boyer, P. D. (1993) *Biochim. Biophys. Acta 1140*, 215−250.
2. Weber, J., and Senior, A. E. (1997) *Biochim. Biophys. Acta 1319*, 19−58.
3. Aggeler, R., Ogilvie, I., and Cappaldi, R. A. (1997) *J. Biol. Chem. 272*, 19621−19624.
4. Noji, H., Yasuda, R., Yoshida, M., and Kinosita, K., Jr. (1997) *Nature 386*, 299−302.
5. Zhou, Y., Duncan, T. M., and Cross, R. L. (1997) *Proc. Natl. Acad. Sci. U.S.A.* 94, 10583−10587.
6. Hasler, K., Engelbrecht, S., and Junge, W. (1998) *FEBS Lett. 426*, 301−304.
7. Yoshida, M., Sone, N., Hirata, H., and Kagawa, Y. (1975) *J. Biol. Chem. 250*, 7910−7916.
8. Tozawa, K., Odaka, M., Date, T., and Yoshida, M. (1992) *J. Biol. Chem. 267*, 16484−16490.
9. Tozawa, K., Miyauchi, M., and Yoshida, M. (1993) *J. Biol. Chem. 268*, 19044−19054.
10. Miwa, K., and Yoshida, M. (1989) *Proc. Natl. Acad. Sci. U.S.A. 86*, 6484−6487.
11. Kagawa, Y., Ohta, S., and Otawara-Hamamoto, Y. (1989) *FEBS Lett. 249*, 67−69.
12. Harada, M., Ohta, S., Sato, M., Ito, Y., Kobayashi, Y., Sone, N., Ohta, T., and Kagawa, Y. (1991) *Biochim. Biophys. Acta 1056*, 279−284.
13. Matsui, T., and Yoshida, M. (1995) *Biochim. Biophys. Acta 1231*, 139−146.
14. Shirakihara, Y., Leslie, A. G. W., Abrahams, J. P., Walker, J. E., Ueda, T., Sekimoto, Y., Kambara, M., Saika, K., Kagawa, Y., and Yoshida, M. (1997) *Structure 5*, 825−836.
15. Abrahams, J. P., Leslie, A. G. W., Lutter, R., and Walker, J. E. (1994) *Nature 370*, 621−628.
16. Cross, R. L. (1988) *J. Bioenerg. Biomembr. 20*, 395−406.
17. Knowles, J. R. (1980) *Annu. Rev. Biochem. 49*, 877−919.
18. Fersht (1985) in *Enzyme Struture and Mechanism* (Freeman, W. H., Ed.) p 236, New York.
19. Herschlag, D., and Jencks, W. P. (1987) *J. Am. Chem. Soc. 109*, 4665−4674.
20. Weber, J., Hammond, S. T., Wilkes-Mounts, S., and Senior, A. E. (1998) *J. Biol. Chem. 37*, 608−614.
21. Hiller, R., and Carmeli, C. (1985) *J. Biol. Chem. 260*, 1614−1617.
22. Chasteen, N. D. (1981) in *Biological Magnetic Resonance* (Berliner, L. J., and Reuben, J., Eds.) Vol. 3, pp 53−119, Plenum Press, New York.
23. Houseman, A. L. P., Morgan, L., LoBrutto, R., and Frasch, W. D. (1994) *Biochemistry 33*, 4910−4917.
24. Houseman, A. L. P., LoBrutto, R., and Frasch, W. D. (1995) *Biochemistry 34*, 3277−3285.
25. Buy, C., Matsui, T., Andrianambinintsoa, S., Sigalat, C., Girault, G., and Zimmermann, J.-L. (1996) *Biochemistry 35*, 14281−14293.
26. Tozawa, K., Odaka, M., and Yoshida, M. (1992) *J. Biol. Chem. 267*, 16484−16490.
27. Tozawa, K., Sekino, N., Yagi, H., Yoshida, M., and Akutsu, H. (1995) *FEBS Lett. 376*, 190−194.
28. Bonvoisin, J., Blondin, G., Girerd, J. J., and Zimmermann, J. L. (1992) *Biophys. J. 61*, 1076−1086.
29. Höfer, P., Grupp, A., Nebenführ, H., and Mehring, M. (1986) *Chem. Phys. Lett. 132*, 279−282.
30. Astashkin, A. V., Dikanov, S. A., and Tsvetkov, Y. D. (1985) *J. Struct. Chem. 100*, 6057−6063.
31. Flanagan, H. L., and Singel, D. J. (1987) *J. Chem. Phys. 87*, 5606−5616.
32. Reijerse, E. J., Shane, J., de Boer, E., Höfer, P., and Collison, D. (1991) in *Electron Magnetic Resonance of Disordered Systems* (Yordanov, N. D., Ed.) pp 253−271, World Scientific, Singapore.
33. Dikanov, S. A., Samoilova, R. I., Smieja, J. A., and Bowman, M. K. (1995) *J. Am. Chem. Soc. 117*, 10579−10580.
34. Astashkin, A. V., Dikanov, S. A., and Tsvetkov, Y. D. (1984) *J. Struct. Chem. 25*, 45.
35. Girault, G., Berger, G., Galmiche, J. M., and André, F. (1988) *J. Biol. Chem. 263*, 14690−14695.
36. LoBrutto, R., Hamstra, B. J., Colpas, G. J., Pecoraro, V. L., and Frasch, W. D. (1998) *J. Am. Chem. Soc. 120*, 4410−4416.
37. Huang, W., Jia, J., Cummings, J., Nelson, M., Schneider, G., and Lindqvist, Y. (1997) *Structure 5*, 691−699.

BI9910732